Research Article

Syed Muhammad Salman*, Safina Razzaq, Muhammad Adnan, Rozina, Sabiha Sultana, Asif Kamal, Abdullah Ahmed Al-Ghamdi, Dunia Abdel Aziz Al Farraj, and Wajid Zaman*

# Green adsorbents for water remediation: Removal of Cr(VI) and Ni(II) using *Prosopis glandulosa* sawdust and biochar

https://doi.org/10.1515/gps-2024-0197
received September 08, 2024; accepted December 15, 2024

**Abstract:** Potentially toxic elements like $Cr^{+6}$ and $Ni^{+2}$ cause severe health hazards. Therefore, the current work was aimed at cleaning water using *Prosopis glandulosa* raw sawdust (SD) and its derived biochar (AC). Both the adsorbents were characterized via SEM, FTIR spectroscopy, EDX, and TGA and were applied for the effective removal of Ni(II) and Cr(VI) at optimum values of experimental conditions, and the mechanism was assessed via adsorption isotherm and kinetic models. The correlation coefficient $R^2$ confirmed pseudo-second-order kinetics and preferred Freundlich isotherm model. Maximum removal of Cr(IV) was obtained at a pH of 4.0, a bio-sorbent concentration of 0.8 $g{\cdot}L^{-1}$, and a temperature of 50°C for 50 min with a metal concentration of 110 ppm, while maximum removal of Ni(II) was obtained for a contact time of 70 min with a metal concentration of 130 ppm in the above-mentioned experimental conditions. The results of the isotherms and kinetic model revealed that metal adsorption processes involved multilayer formation on the biosorbent's heterogeneous surface. Also, their thermodynamic investigation showed that the adsorption process is spontaneous and exothermic and, therefore, can be effectively utilized to remove Cr and Ni from water.

**Keywords:** potentially toxic elements, *Prosopis glandulosa*, adsorption study, isotherm models, kinetic study, batch experiment

## 1 Introduction

Pollutants like potentially toxic elements in an aquatic ecosystem are a foremost worldwide issue. Due to the massive industrialization that has increased in recent years, industry waste containing pollutants, including potentially toxic elements, pharmaceutical effluents, and organic dyes, are released into natural waterways, endangering the health of people, animals, and plants [1]. The health of organisms is seriously threatened by the release of these potentially toxic elements into the aqueous system from various anthropogenic sources [2,3]. Among various pollutants, HMs are the top cause of environmental pollution because they cannot degrade easily and enter human bodies through the food chain [4]. It is difficult to remove heavy metal ions Ni and Cr from aquatic systems because of their small, non-biodegradable, and highly stable nature [5]. Potentially toxic elements, like Ni(II) and Cr(VI), are regarded to be the most hazardous type of pollutant [6].

Chromium (Cr) is applied in the textile and steel industry, leather lashing, and coloring glass as catalysts, anti-corrosives, and oxidizing agents [7]. Many isotopes of chromium cause different biomedical complications. The powder of Cr metal is a fire threat. All Cr(VI)-containing chemical compounds are mutagenic, carcinogenic, and life-threatening to all forms of biodiversity. Cr(VI) is highly toxic due to its strong oxidizing nature. On entering the blood, Cr(VI) causes serious damage to the blood cells, kidneys, and liver, resulting in renal failure, liver failure, and hemolysis [8]. Several allergenic effects of Cr have also been reported in humans. Many species of living organisms require nickel (Ni) in a trace amount [9]. Nickel-deficient food results in

*** Corresponding author: Syed Muhammad Salman,** Department of Chemistry, Islamia College Peshawar, Peshawar, Pakistan, e-mail: salman@icp.edu.pk
*** Corresponding author: Wajid Zaman,** Department of Life Sciences, Yeungnam University, Gyeongsan, 38541, Republic of Korea, e-mail: wajidzaman@yu.ac.kr
**Safina Razzaq, Rozina, Sabiha Sultana:** Department of Chemistry, Islamia College Peshawar, Peshawar, Pakistan
**Muhammad Adnan:** Assistant Manager Iqbal Ahmad Qarshi Laboratory, Qarshi Industry, Hattar, Haripur, Pakistan; Department of Chemistry, Bacha Khan University, Charsadda, Pakistan
**Asif Kamal:** Department of Plant Sciences, Faculty of Biological Science, Quaid-i-Azam University, Islamabad, 4520, Pakistan
**Abdullah Ahmed Al-Ghamdi, Dunia Abdel Aziz Al Farraj:** Department of Botany and Microbiology, College of Science, King Saud University, P.O. 2455, Riyadh, 11451, Saudi Arabia

liver hepatic problems in rats and chicks. Enzymes and microorganisms also require Ni for their normal functioning. Along with biological applications, it is also used in batteries, electroplating, anti-corrosives, and as a catalyst. Its alloy tubing is used as a protective coat in the purification of plants. Ni compounds are considered carcinogens in the human body. Cigarette smoke and skin contact with jewelry and scrubbing agents is a direct source of Ni intake by humans. Ni causes bronchitis, lung cancer, lung fibrosis, bronchoconstriction, and birth dermatitis [10].

Currently, membrane separation, chemical coagulation, ion exchange, precipitation, activated sludge, flocculation, and photodegradation are just a few of the purification techniques used for heavy metal remediation [11]. The removal of HMs from aqueous media can be accomplished through conventional methods such as solvent adsorption, extraction, membrane separation, chemical precipitation, and ion exchange. Adsorption is a more effective technique than others for degrading HMs from contaminated water because of its high efficacy and cost-effectiveness [12]. Incorporating phyto-based green technology in the degradation of HMs from polluted water offers several benefits. Aquatic plants can serve as natural absorbers of other pollutants and potentially toxic elements. The most economical and effective method for removing impurities from wastewater is to use aquatic plants [13]. In recent times, aquatic plants have been widely utilized to remove pollutants and HMs from water. Emergent aquatic plants are efficient in amassing metals in their internal parts, which leads to metal uptake by the plants [14]. However, the use of plant-based green technology in HM remediation is a time-consuming process. Therefore, the quick and easy way to prepare plant-based materials for the effective removal of HMs can be an alternative to save time.

Biochar serves as a biosorbent obtained through pyrolysis of a variety of biomass-based substances [15]. It is obtained from biomass via multiple carbonization ways of the biomass [16]. Biochar is also referred to as pyrogenic black carbon-rich material and has desirable properties such as high permeability, porosity, and a large surface area. Aside from these characteristics, the different functional groups make it a desirable choice for adsorbing numerous HMs over the outermost layer, resulting in efficient wastewater disposal [17]. Biochar is an economical and eco-friendly approach and it can be applied for multiple purposes, like waste management, soil remediation, greenhouse gas declination, plant growth, and production of energy. Due to a large number of benefits in various fields of life, biochar is often termed as “Black Gold” [18]. Biochar can be prepared from different sources. Among them, plant biomass is extensively applied for biochar synthesis due to their environmental friendliness, economical nature, abundant natural constituents, and excellent biosorption ability [19]. The synthesized adsorbent, derived from *Prosopis glandulosa* sawdust (SD) and its biochar, offers an environmentally friendly solution by utilizing abundant, renewable biomass that would otherwise go to waste. This approach not only reduces environmental impact but also provides a cost-effective alternative to commercially available adsorbents, minimizing the need for expensive raw materials.

This work presents a comprehensive use of *Prosopis glandulosa* raw SD and its derived biochar as effective, low-cost adsorbents for the removal of potentially toxic elements $Cr^{6+}$ and $Ni^{2+}$ from aqueous solutions. This study begins with a detailed characterization of both adsorbents using SEM, FTIR spectroscopy, EDX, and TGA to understand their surface properties and structures. A series of batch experiments were conducted to assess the optimal conditions for metal adsorption, including pH, biosorbent concentration, temperature, and contact time. The adsorption mechanisms were analyzed using adsorption isotherms and kinetic models, with the results indicating that both adsorbents followed pseudo-second-order kinetics and the Freundlich isotherm model, suggesting multilayer adsorption on the heterogeneous surface of the biosorbents. Thermodynamic analysis revealed that the adsorption process is spontaneous and exothermic, further validating the suitability of these biosorbents for environmental remediation. The study concludes that SD and active carbon (AC) are promising, environmentally friendly alternatives for the effective removal of Cr and Ni from contaminated water, with potential for large-scale application in water treatment.

The current study brings innovation by introducing *Prosopis glandulosa* raw SD and its derived biochar as cost-effective and environmentally friendly adsorbents for removing the toxic heavy metals $Cr^{6+}$ and $Ni^{2+}$ from contaminated water. Unlike conventional water treatment methods, which often involve expensive and complex technologies, this study focuses on utilizing a low-cost, sustainable material that is widely available and can be easily converted into biochar, enhancing its adsorption capacity. The study employs thorough characterization techniques and rigorous experimental analysis to determine optimal conditions for the maximum removal of both metals. By applying pseudo-second-order kinetics and Freundlich isotherm models, this study provides deeper insights into the adsorption mechanism, revealing multilayer diffusion on the adsorbent’s surface. Thermodynamic analysis further confirms the process as spontaneous and exothermic, which suggests its viability for large-scale applications. The

problem statement centers around the need for efficient, low-cost methods to treat water contaminated by $Cr^{6+}$ and $Ni^{2+}$, which pose serious health risks. The objectives of the study include evaluating the adsorption efficiency of SD and AC, optimizing experimental conditions, and understanding the adsorption dynamics. The prospects include scaling up this method for industrial water treatment, exploring its application to other toxic metals, and further enhancing the biosorbent's performance for broader environmental remediation.

# 2 Materials and methods

## 2.1 Chemicals

For the examination of Ni(II) and Cr(VII) adsorption, nickel sulfate hexahydrate [$NiSO_4(H_2O)_6$] 99%, potassium chromate [$K_2Cr_2O_4$] 99%, HCl 35%, and $H_2SO_4$ 98% were purchased from Sigma-Aldrich, Germany, and utilized in the experiment.

## 2.2 Collecting plant stem

The stem of the *Prosopis glandulosa* plant was sourced from Hayatabad, Peshawar, Pakistan. To eliminate moisture, the stem was air-dried for at least 4 days. The outer layer of the dried stem was then peeled off to prevent any impurities from contaminating the final sample. The peeled stem was then chopped into small pieces, crushed, and sieved after grinding to obtain a powder with an approximate size of 1 mm. The prepared material was stowed in airtight bottles, with half designated for use as an adsorbent and the remaining portion reserved as a precursor for the second adsorbent.

## 2.3 Preparation of AC

An electric boiler with a N2 inlet and multiple gas outlets was used to char approximately 100 g of SD. The furnace temperature was first raised to 400°C at a rate of 10°C·min$^{-1}$, and the substance was carbonized for about an hour in an inert nitrogen environment. The temperature was extended to the desired activation temperature of 800°C; at that point, a syringe pump delivered steam and N2. The furnace was turned off after 1 h of keeping the process isothermal.

Once at room temperature, the sample was cleaned with 0.05 M HCl to remove any ash from the substance. It was subsequently washed in distilled water. Following washing, the rest of the mass was dried in a heated oven at 105°C for 6 h, yielding biochar, which is also known as activated carbon.

## 2.4 Characterization of adsorbents

The adsorbents, including the prepared AC and SD, were characterized systematically via microscopic and spectroscopic techniques. The functional groups were assessed by FTIR spectroscopy (PerkinElmer, Spectrum RX I), SEM (SEM, JEOL JSM 6390) was performed for investigation of surface morphology, EDX (Oxford Instruments, Concord, MA) was performed to analyze the elemental composition, and thermal properties were assessed using a TGA (Mettler, Toledo 851).

## 2.5 Batch experiment

Approximately 40 mL of heavy metal solutions with concentrations ranging from 20 to 200 mg·L$^{-1}$ was blended with 0.08 g of SD and AC. The concentrations of these solutions were determined using an atomic absorption spectrophotometer (PerkinElmer USA-700 AAS). The adsorption ability of Ni(II) and Cr(VI), denoted as $q_i$ (mg·g$^{-1}$), and the percentage remediation ($R$%) were premeditated using the following formula [20]:

$$q_i = (C_i - C_f) \times \frac{V}{M} \quad (1)$$

$$\% R = \frac{C_i - C_f}{C_i} \times 100 \quad (2)$$

where $C_i$ is the initial concentration of metals, $C_f$ is the concentration of metals at the final stage, $V$ is the whole volume of the mixture, and $M$ is the adsorbent mass.

Isotherm models are utilized to explain the adsorption mechanism and the interactions between the metal and adsorbent. Consequently, the adsorption statistics were studied using the Freundlich and Langmuir models.

## 2.6 Biosorption kinetics

The kinetics of a reaction are critical in evaluating a batch adsorption experiment because they provide data about the sorption rate. As a result, data from multiple experiments were analyzed to determine the kinetics of the metals Ni(II) and Cr(VI) under consideration. Lindegren's pseudo-first-order model and pseudo-second-order kinetic model were used to evaluate the kinetics data.

### 2.7 Assessment of the effect of metal dosage

To assess the influence of Cr and Ni concentration on the adsorption method, solutions with different amounts, including 10, 30, 50, 70, 90, 110, 130, 150, 170, and 190 ppm, were synthesized. Under neutral conditions, 0.08 g of AC and SD adsorbents were included to differentiate sets of all these effective solutions. In order to optimize the interaction between the metal and adsorbent surface, samples were stirred at 200 rpm for 2 h using an orbital shaker. Next, the solutions were filtered and examined with an atomic absorption spectrophotometer.

### 2.8 Effect of adsorbent dose on metal adsorption

A series of solutions with identical metal ion concentrations were prepared, particularly 110 ppm for Cr(VI) and 130 ppm for Ni(II). Adsorbent quantities that varied from 0.02 to 0.2 g for each AC and SD were mixed with a particular metal-containing water solution individually, while the remaining parameters remained constant. Before the filtration process, the samples were shaken for 2 h at 200 rpm to ensure that metal ions adhered to the adsorbent completely. The obtained filtrate solutions were investigated using an atomic absorption spectrophotometer, and the results are presented graphically.

### 2.9 Time interaction effect

For optimal optimization of the interaction time, various periods of shaking durations for contact between the adsorbate and adsorbent were selected, which varied from 10 to 150 min with 10-min intervals. This applies to every metal ion aqueous solution while maintaining other factors constant. Then, the samples were filtered, and the filtrate was analyzed using an atomic absorption spectrophotometer.

### 2.10 Effect of pH on HM adsorption

To investigate the impact of pH under optimal conditions for experiments, solutions containing 110 ppm Cr(VI) and 130 ppm Ni(II) were prepared. A pH value between 2 and 10 was chosen for adjustment. The pH of the solutions was adjusted with $H_2SO_4$ and NaOH. Adsorbent (0.08 g) was added to each solution individually and shaken at 150 rpm to ensure maximum interaction time. A spectrophotometer with atomic absorption was used to analyze the filtrates obtained after shaking.

### 2.11 Effect of temperature on HM adsorption

To investigate the effect of changing the heat content on adsorption while keeping the other parameters constant, temperature ranges from 25°C to 50°C were chosen, with the remaining parameters adjusted.

## 3 Results and discussion

### 3.1 FTIR spectroscopy

Before the adsorption study, the prepared AC and SD were assessed through FTIR spectroscopy to analyze multiple functional groups. Different functional groups were observed both in AC and SD, as shown in Figure 1a and b. FTIR spectroscopy of SD showed different peaks at 3,332, 2,884, 1,736, 1,634, 1,232, 1,191, 1,031, and 513 $cm^{-1}$. These peaks correspond to the primary amine, $CH_2$ bonding in the aliphatic compound, C═O ester, C–C stretch alkenes, C–N stretch of amine, C–O–C due to the presence of polysaccharides, P–O–C stretching, and C–C stretching in the aromatic ring, respectively. These findings are aligned with the work of previous researchers [21]. Similarly, the FTIR spectra of AC revealed eight dominant peaks at 2,925, 2,157, 1,778, 1,591, 1,504, 1,094, 908, and 716 $cm^{-1}$ [22]. The peaks observed at 2,925 and 2,157 $cm^{-1}$ confirm the presence of CH and $CH_2$ aliphatic and Se–O bonds, respectively, while the peaks at 1,778, 1,591, and 1,504 $cm^{-1}$ are assigned to C═C stretching, C═O functional groups, and C–C stretching [23]. The peaks at 1,094, 908, and 716 $cm^{-1}$ correspond to C–N bonding, symmetric C–O–C stretching, and P–O bonding [24].

### 3.2 SEM and EDX analysis

SEM was performed to understand the surface texture of the adsorbents. Adsorbents with a higher porosity have a larger surface area for adsorption. SEM images reveal that the surface particles are dispersed irregularly, resulting in a rough and porous texture, which makes it ideal for the adsorption processes [25]. The SEM results of SD (Figure 2a and b) and AC (2c and d) are presented in Figure 2. EDX was performed to assess the elemental composition. The EDX results confirmed the presence of calcium, potassium, carbon, oxygen, chlorine, sulfur, and nitrogen in the

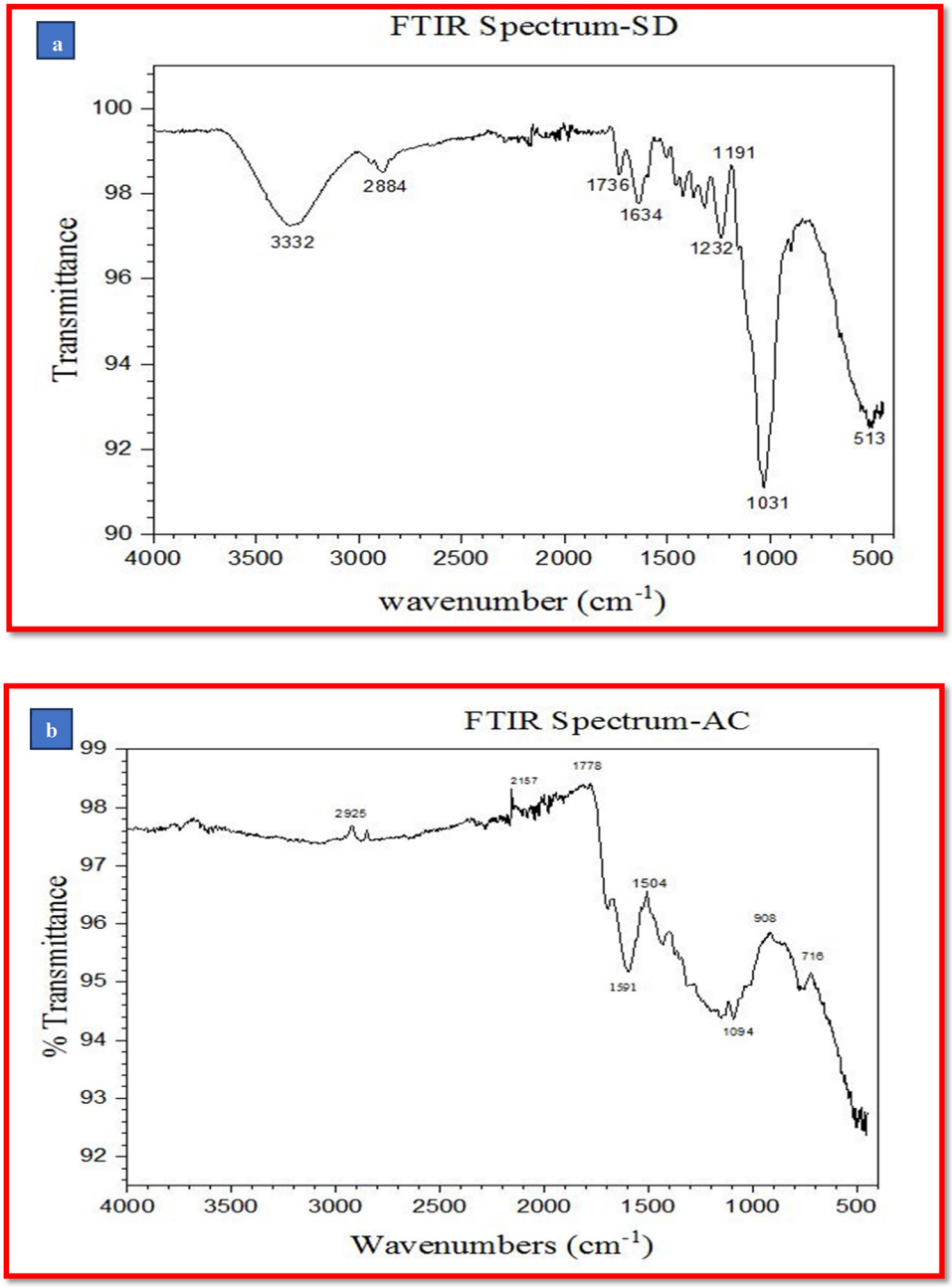


**Figure 1:** FTIR spectra of SD (a) and AC (b) of *Prosopis glandulosa* stem.

adsorbent. The EDX spectra, along with the elemental composition of SD and AC, are shown in Figures 3 and 4. These findings are consistent with the work of Singh et al. [26].

## 3.3 TGA

TGA was performed to assess the heat-bearing properties and ranges of biomass [27]. TGA revealed that mass decreases with increasing temperature. The earlier weight loss at an initial temperature corresponds to the removal of water content in the particle surface [28]. This curve was produced because of the loss of water (50–100°C), and weight loss because of the removal of cellulose and hemicellulose (200–400°C). It has been observed that SD has low thermal stability in comparison to AC (Figure 5a and b). These results confirmed the excellent thermal properties of both SD biochar and AC.

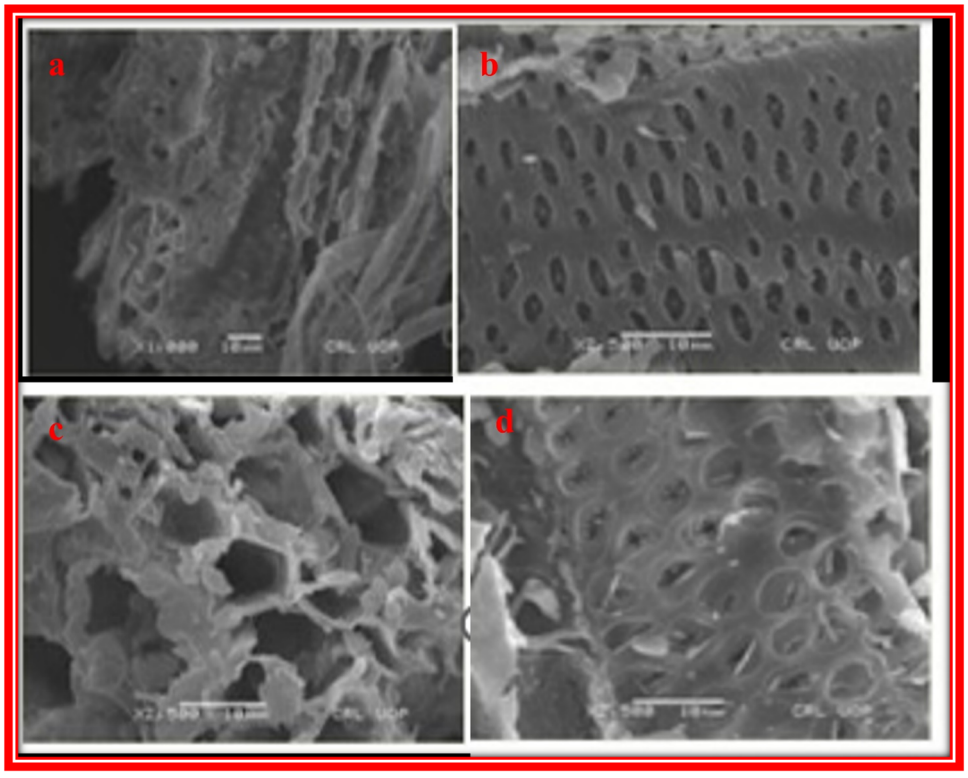


**Figure 2:** SEM images of SD (a and b) and AC (c and d).

## 3.4 Batch adsorption experiment

The adsorption experiments evaluated the optimal adsorption parameters under various experimental conditions. In the current experiment setup, the effect of modification in the pH of solution, dose of adsorbent, dose of adsorbate, and interaction time on the adsorption efficacy was investigated.

### 3.4.1 Effect of metal dosage on absorption

The adsorption process was examined with solutions of chromium and nickel metal ions at concentrations of 10, 30, 50, 70, 90, 110, 130, 150, 170, and 190 ppm. During this process, 0.08 g of SD and AC adsorbents were added. In the case of AC, the highest adsorption value for Cr(VI) was 110 ppm, and that for Ni(II) was 130 ppm at the $C_i$. No further

| Element | Weight% | Atomic% |
|---|---|---|
| C K | 61.12 | 67.47 |
| N K | 10.10 | 9.56 |
| O K | 26.93 | 22.32 |
| P K | 0.16 | 0.07 |
| S K | 0.17 | 0.07 |
| Cl K | 0.19 | 0.07 |
| K K | 0.76 | 0.26 |
| Ca K | 0.57 | 0.19 |
| Totals | 100.00 | |

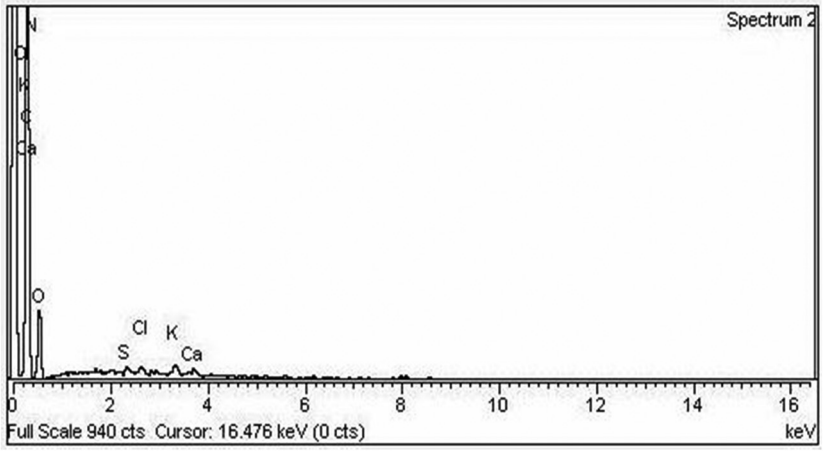


**Figure 3:** EDX spectra of SD.

| Element | Weight% | Atomic% |
|---|---|---|
| C K | 83.60 | 88.96 |
| O K | 11.87 | 9.48 |
| Si K | 0.27 | 0.12 |
| P K | 0.35 | 0.14 |
| S K | 0.38 | 0.15 |
| K K | 1.90 | 0.62 |
| Ca K | 1.63 | 0.52 |
| Totals | 100.00 | |

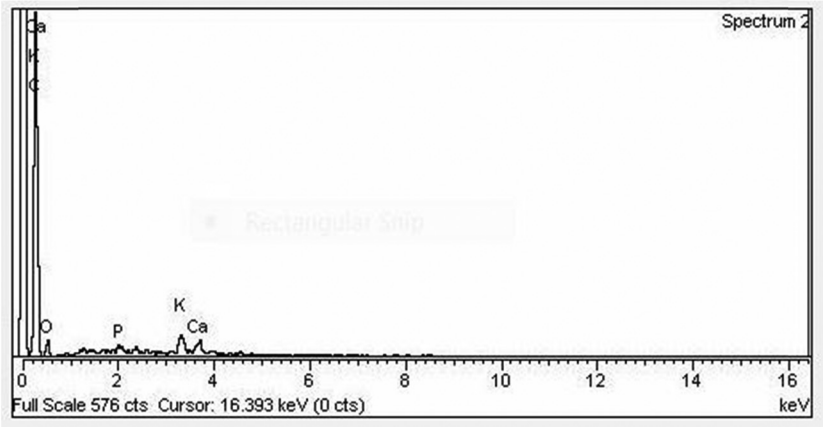


**Figure 4:** EDX spectra of AC.

increase was examined as all the active sites on the surface of AC and SD were fully saturated, leaving no remaining free sites for metal adsorption [29]. All these results are depicted in Figure 6a and b.

### 3.4.2 Effect of adsorbent dose

The highest adsorption potential was obtained at 0.08 g of adsorbents (AC and SD) against Cr(VI) and Ni(II), as depicted in Figure 7a and b. With further increase in the concentration of adsorbent, no increase was examined, indicating that all the pores on the surface were entirely loaded, having no further sites for the attachment of the metal with the adsorbent [30]. Our results are aligned with a previous study [31].

### 3.4.3 Effect of time of interaction

The effect of time of interaction on adsorption is crucial, as it determines the extent to which adsorbates can adhere to the surface [32]. To optimize the interaction time between the adsorbent and the adsorbate, various shaking durations were tested, ranging from 10 to 150 min in 10-min intervals. These tests were conducted on each metal ion solution while maintaining all other parameters constant. Maximum adsorption for Cr(VI) was reached at 50 min,

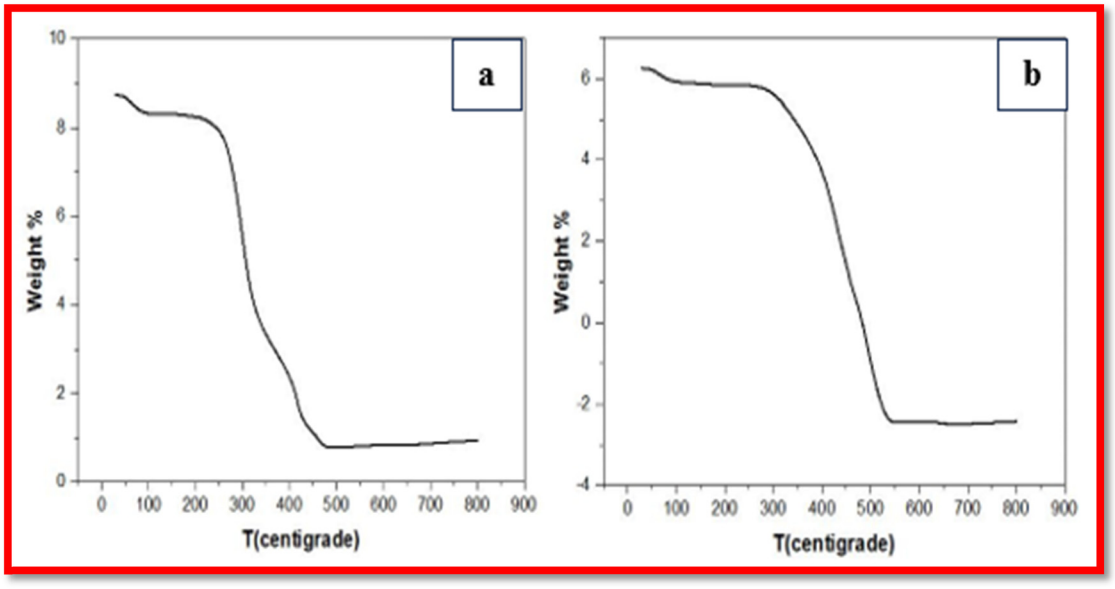


**Figure 5:** TGA for SD (a) and AC (b).

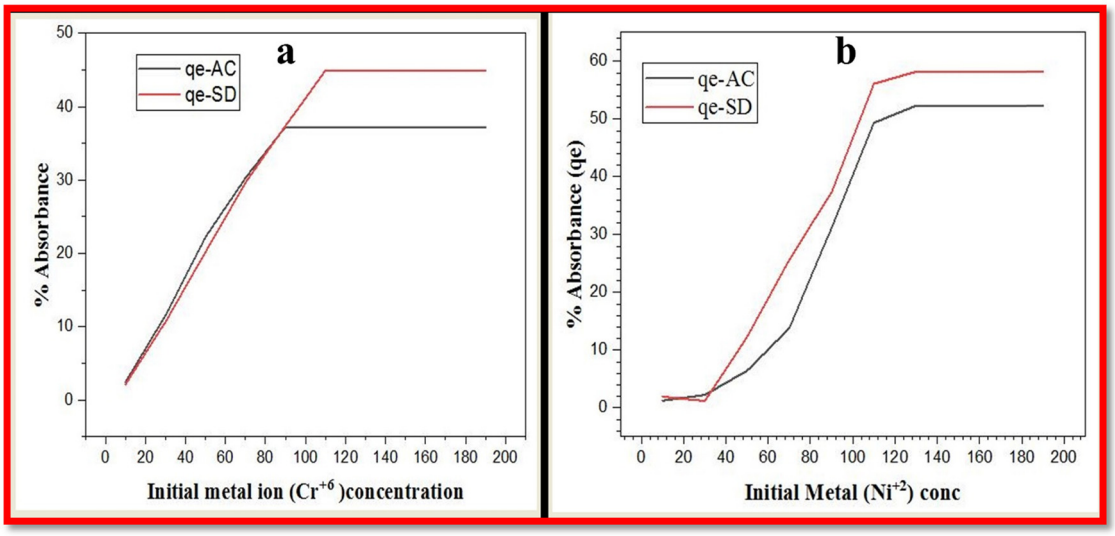


**Figure 6:** Effect of Cr(VI) (a) and Ni(II) (b) concentration on the adsorption potential of SD and AC.

while that of Ni(II) was at 70 min with AC. In contrast, SD required a longer interaction time to achieve effective adsorption. The whole results are depicted in Figure 8a and b. With the passage of time, the surface sites on the adsorbent are fully occupied by the metals, which cause a reduction in the adsorption of Ni(II) and Cr(VII) [33].

### 3.4.4 Effect of pH

The pH of the solution plays a crucial role in the adsorption process, as it influences the surface charge of the adsorbent and the ionization state of the adsorbate. At the pH zero charge, where the adsorbent's surface has no net charge, the adsorption efficiency of metal ions can either increase or decrease depending on the pH, as it affects both electrostatic interactions and the availability of adsorption sites [34]. The effect of pH on metal elimination is shown in Figure 9. The absorption of metals was assessed at acidic and alkaline pH. During pH optimization, the highest adsorption of Cr(VI) was observed at pH 4, while for Ni(II), the optimal pH was also 4. This indicates that the adsorbent's active sites were saturated with hydrogen ions, leaving no available sites for the adsorbate to attach [35]. Additionally, at higher pH, the OH ions were precipitated, which caused the reduction of the absorption capacity [36]. The presence of interfering ions can significantly affect the adsorption capacity of biosorbents by competing with

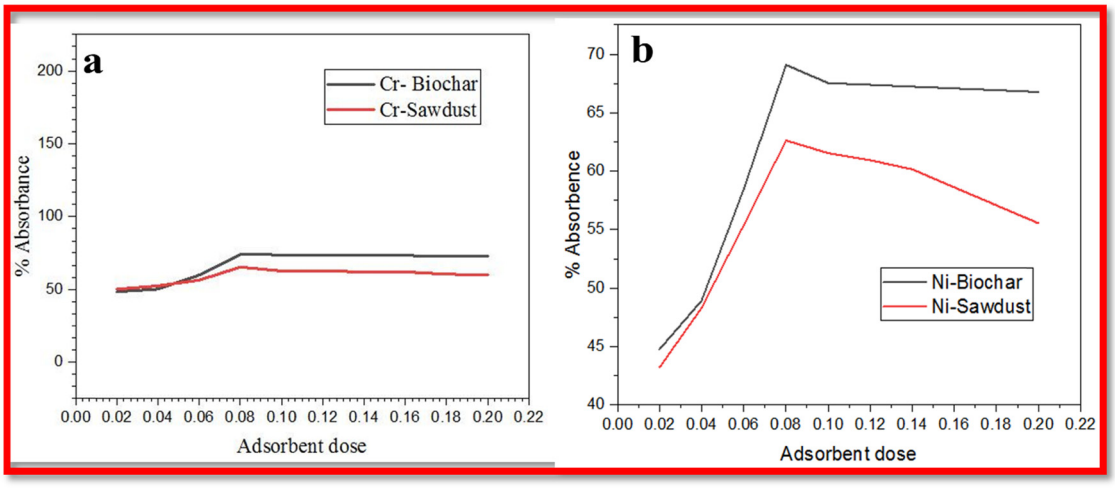


**Figure 7:** Effect of adsorbent concentration for the adsorption of Cr(VI) (a) and Ni(II) (b) on SD and AC.

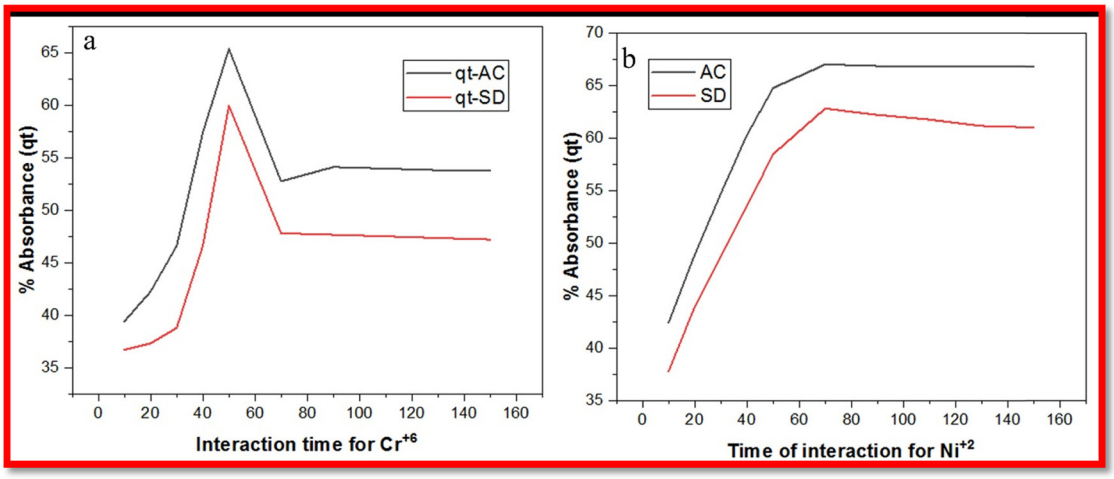


**Figure 8:** Impact of interaction times for Cr(VI) (a) and Ni(II) (b) adsorption on SD and AC.

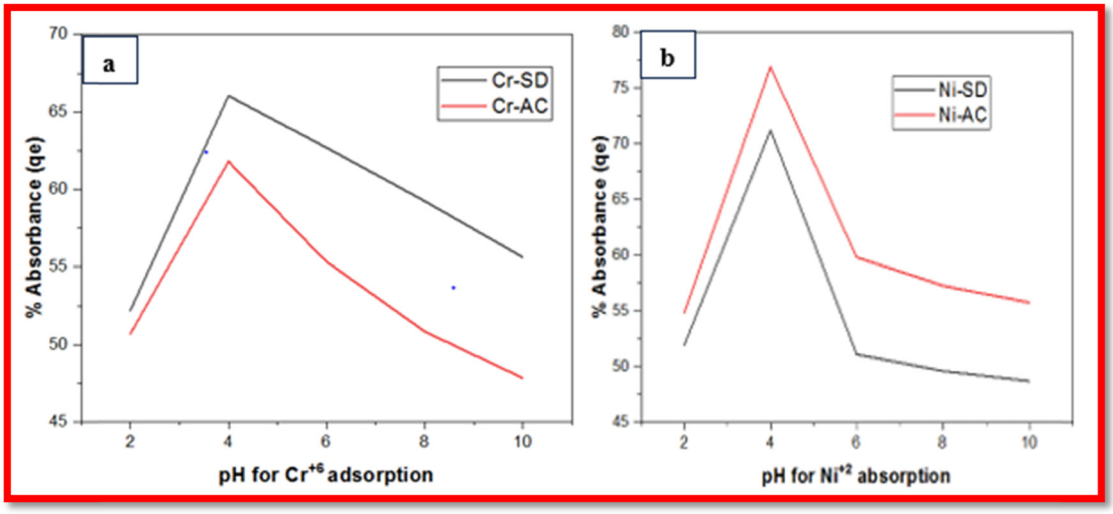


**Figure 9:** Effect of pH on $Cr^{+6}$ (a) and $Ni^{+2}$ adsorption by SD and (b) AC.

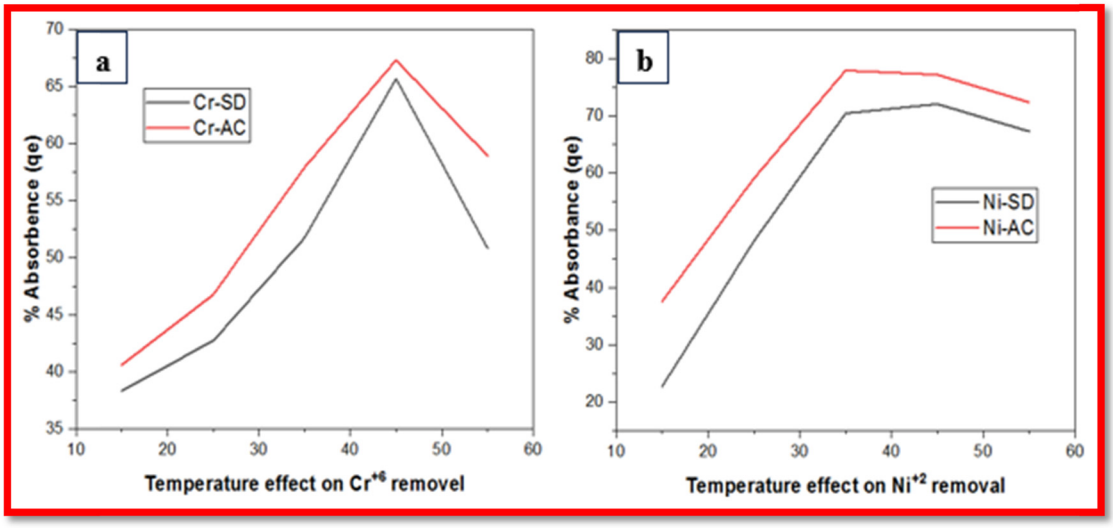


**Figure 10:** Comparison of temperature effects for Cr(VI) (a) and Ni(II) (b) adsorption on SD and AC.

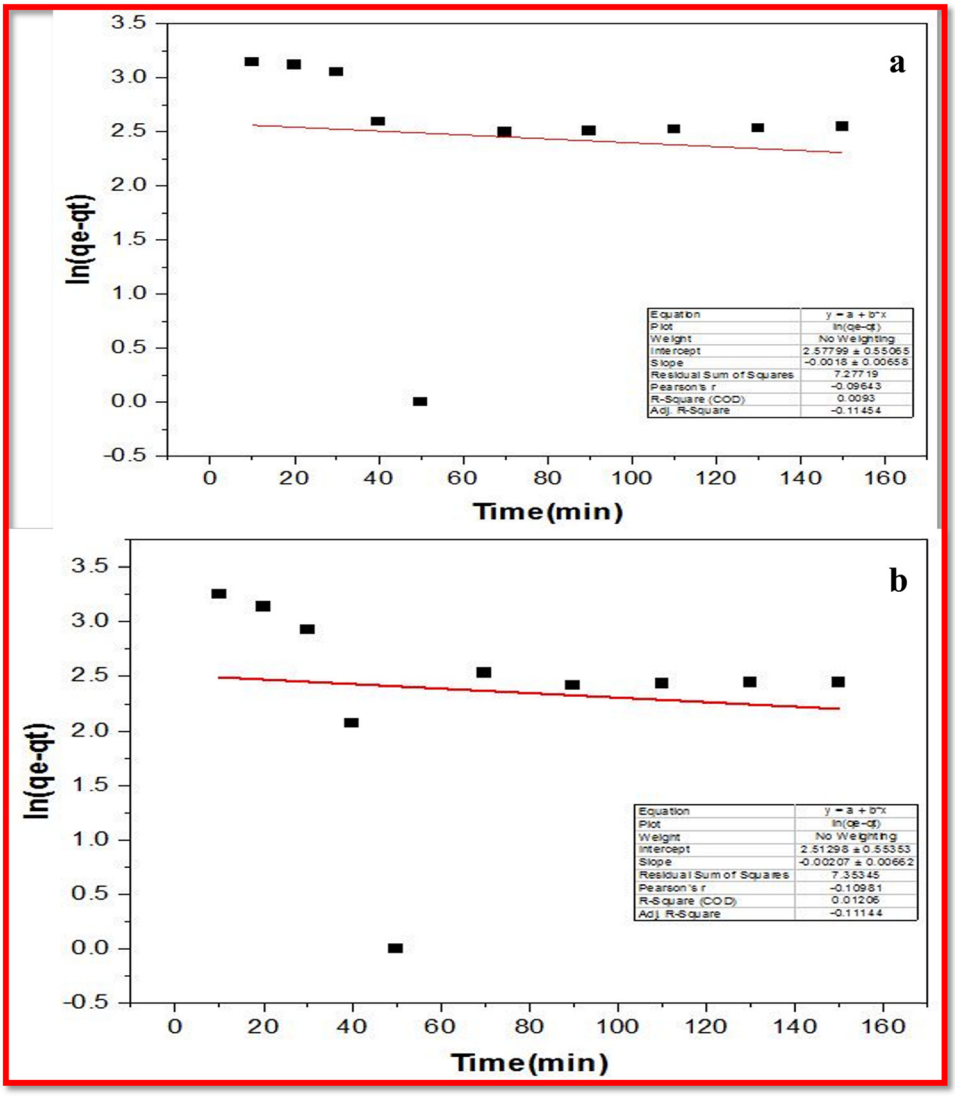


**Figure 11:** Pseudo-first-order kinetics for the adsorption of $Cr^{6+}$ on SD (a) and AC (b).

target ions for active sites on the adsorbent surface, leading to reduced efficiency. Understanding the effects of these ions is crucial for optimizing the adsorption process, as they can alter the adsorption rate and the overall effectiveness of the treatment method.

#### 3.4.5 Effect of temperature on adsorption efficiency

To assess the effect of varying heat content on adsorption while keeping other parameters constant, temperatures from 25°C to 50°C were selected, with the remaining parameters being optimized. Adsorption increased up to a certain temperature increase but decreased after the optimum limit as the biomass texture changed. With the increase in temperature, the removal of Cr(VI) and Ni(II) improves (Figure 10). The effect of temperature varies across different metals, and each adsorbent's attachment sites respond differently to temperature fluctuations [37].

## 3.5 Adsorption kinetics studies

The kinetics of Cr(VI) and Ni(II) adsorption onto SD and AC were studied. The quantity of metal adsorbed was monitored over time for both Cr and Ni adsorption, as shown in Figures 11a, b, and 12a, b, respectively. Adsorption occurred quickly at first because there were more adsorption sites available. The process gradually slowed down until

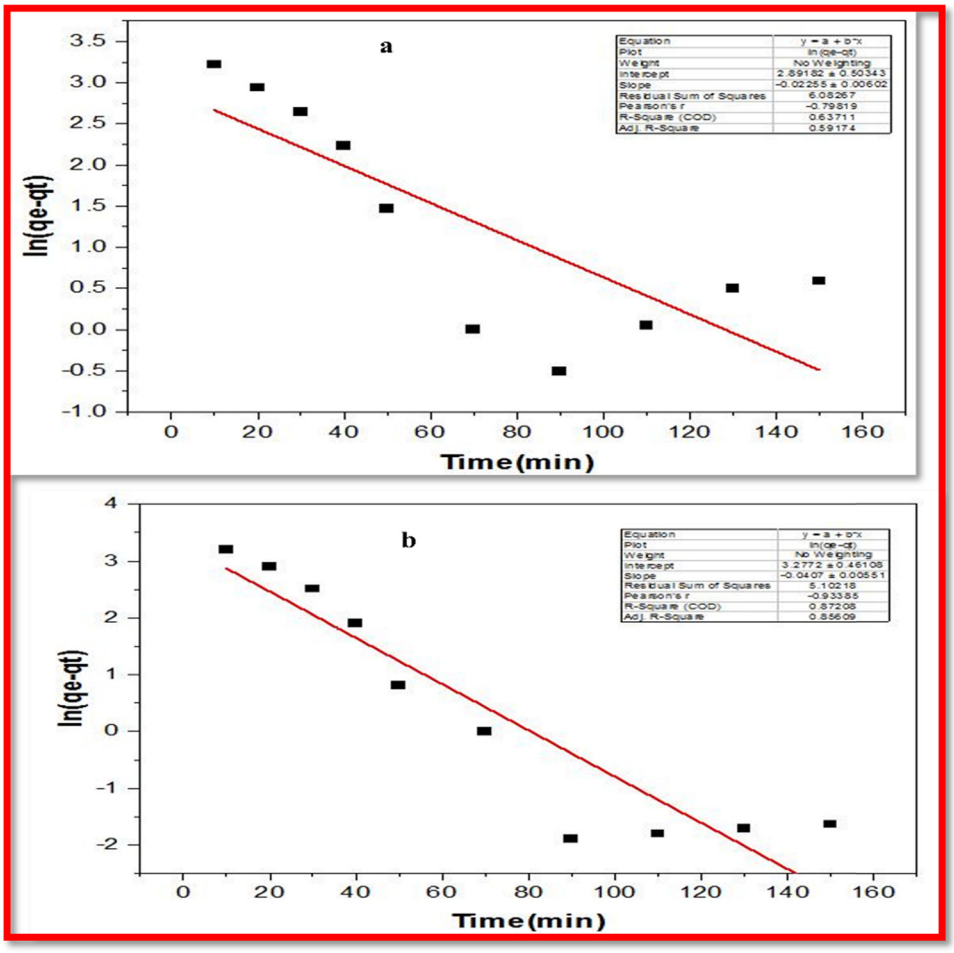


**Figure 12:** Plot of pseudo-first-order adsorption for Ni(II) on SD (a) and AC (b).

equilibrium was reached when the adsorbent's active sites were saturated. Two kinetic models were used to explore the kinetic behavior of current adsorption: pseudo-first order and pseudo-second order [38]. The pseudo-first-order model is commonly used to describe the initial phase of the adsorption under the assumption that the rate of solute uptake over time is directly proportional to the change in saturation concentration and the quantity of solute adsorbed onto the solid.

Table 1 presents the pseudo-first-order parameters for the adsorption of Cr(VI) onto both AC and SD and Table 2 provides these parameters for the adsorption of Ni(II). The adsorption data are related to the pseudo-first-order model using a straight-line equation, where the intercept and slope are derived from plotting ln ($q_e - q_t$) versus time ($t$) and are used to calculate the values of $q_e$ and $k_1$. A similar pattern was examined for Ni and Cr removal previously [39,40]. These data produce a straight line, demonstrating that the pseudo-first-order model is the most appropriate for describing the adsorption process:

$$\ln(q_e - q_t) = \ln(q_e) - k_1 t \quad (3)$$

Pseudo-second-order kinetics is executed by the amount of metal on the surface and the number of ions adsorbed at equilibrium. Pseudo-second-order kinetics was calculated using the following formula:

$$t/q_t = 1/k_2 q_e + 1/q_e(t) \quad (4)$$

where $q_t$ is the adsorption at time $t$, $q_e$ is the adsorption capacity at equilibrium, and $K_2$ is the equilibrium rate constant (g·mg$^{-1}$·min$^{-1}$).

The values of $q_e$ and $k_2$ are represented by the intercept and slope, respectively, while the plot of $t/q_t$ is used to assess the results over time. The $R^2$ values in Tables 3 and 4 indicate that both Cr(VI) and Ni(II) follow pseudo-second-order for adsorption onto both AC and SD derived from the stem of *P. glandulosa*. The pseudo-second-order data for Cr(VI) are presented in Figure 13a and b, and those for $Ni^{2+}$ are presented in Figure 14a and b. The parameters for pseudo-second-order kinetics for Cr(VI) adsorption onto

**Table 1:** Pseudo-first-order data for Cr(VI) adsorption on AC and SD

| Metal | Adsorbent | Intercept $Q_e$ | Slope $K_1$ | $R^2$ |
|---|---|---|---|---|
| $Cr^{6+}$ | SD | 2.57799 | −0.0018 | −0.11454 |
| | Biochar (AC) | 2.51298 | −0.00207 | −0.11144 |

**Table 2:** Pseudo-first-order study for Ni(II) adsorption onto AC and SD

| Metal | Adsorbent | Intercept $Q_e$ | Slope $K_1$ | $R^2$ |
|---|---|---|---|---|
| $Ni^{2+}$ | SD | 2.89182 | −0.02255 | 0.59174 |
| | Biochar (AC) | 3.2772 | −0.0407 | 0.85609 |

both AC and SD are presented in Table 3, and those for $Ni^{2+}$ are presented in Table 4. The data of the pseudo-second-order reaction are aligned with previous work [41].

## 3.6 Isotherm studies

The quantity of metal solution adsorbed onto an adsorbent surface at constant pressure and temperature is graphically represented. Isothermal studies are crucial for determining the adsorption potential of AC and SD for understanding the interaction between the adsorbent and adsorbate. The Freundlich and Langmuir models were applied to determine the isothermal parameters and to elucidate the observed adsorption behavior.

### 3.6.1 Langmuir isotherm model

The Langmuir isotherm model is based on hypotheses that are only applicable to monolayer adsorption [42]. The adsorption sites on the surface of biomass are plane, and there are no forces holding the adsorbed molecules onto

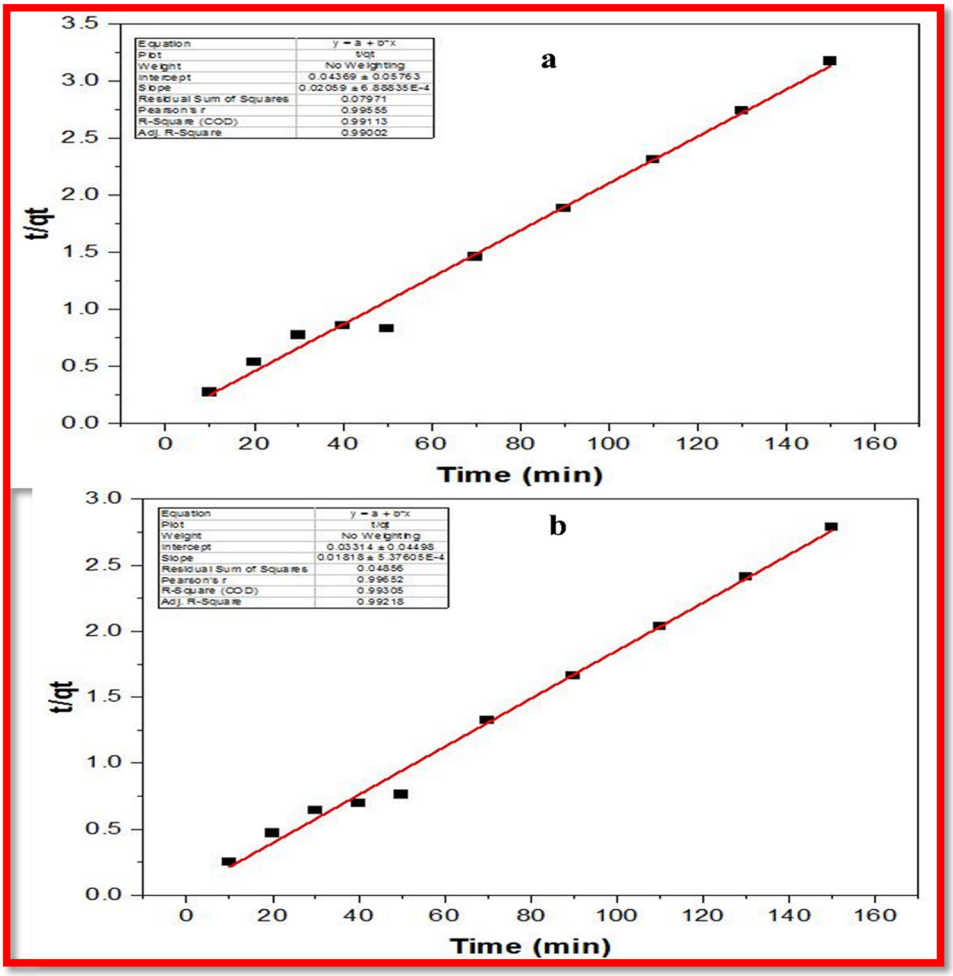


**Figure 13:** The plot of pseudo-second-order adsorption for $Cr^{6+}$ on SD (a) and AC (b).

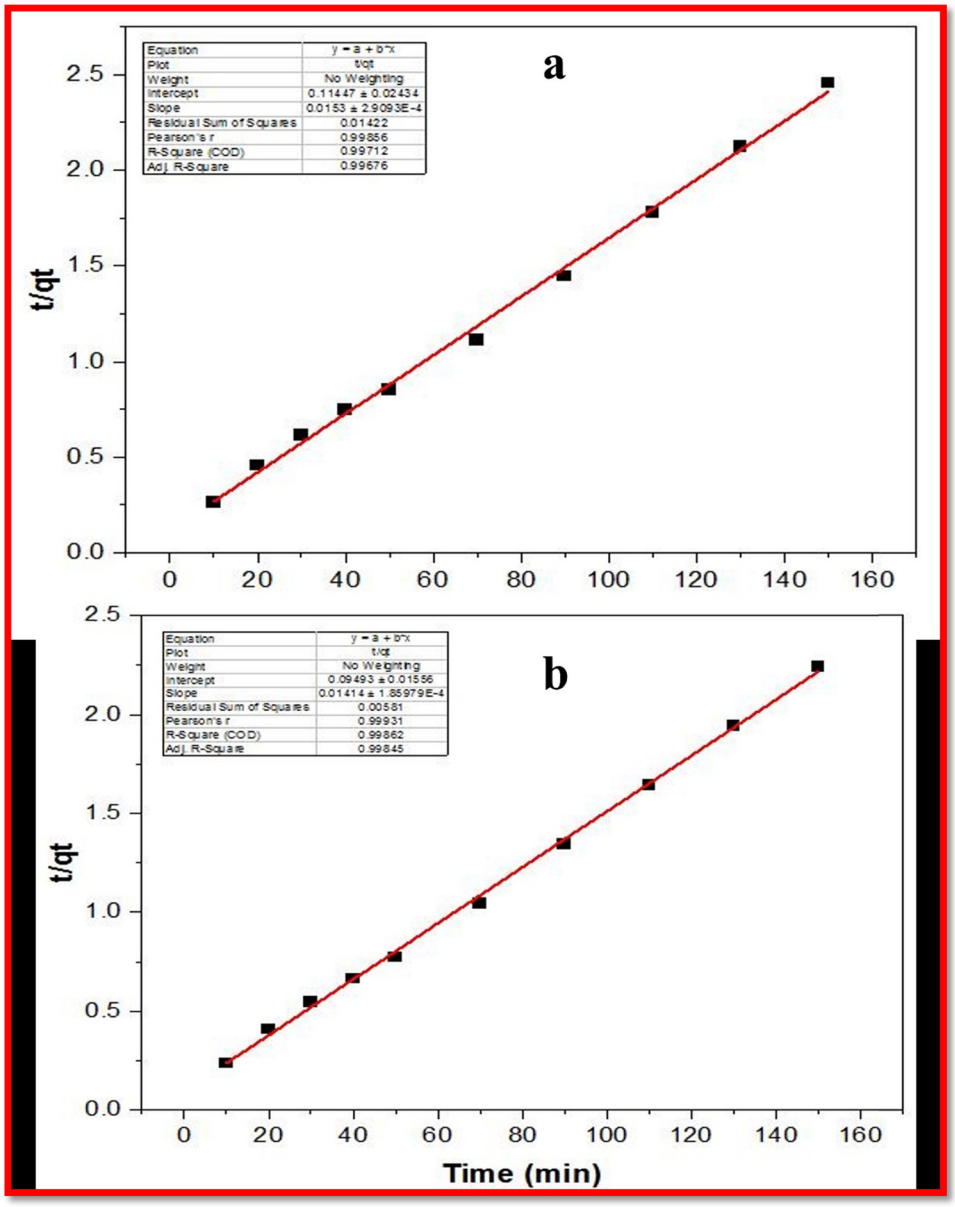


**Figure 14:** Pseudo-second-order study for $Ni^{2+}$ adsorption on SD (a) and AC (b).

the surface. The Langmuir isotherm model was intended using the following equation:

$$Ce/q_e = 1/q_{max}b + Ce/q_{max} \quad (5)$$

where $q_e$ is the adsorption at equilibrium, Ce is the concentration of the adsorbate left unabsorbed, $b$ is the adsorption Langmuir constant, and $q_{max}$ is the maximum efficacy of the adsorbent.

$Ce/q_e$ was plotted against Ce and $b$, and $q_{max}$ was calculated from the slope and intercept values for $Cr^{6+}$ (Figure 15)

**Table 3:** Pseudo-second-order adsorption kinetics for Cr(VI) adsorption on AC and SD

| Metal | Adsorbent | Intercept $Q_e$ | Slope $K_2$ | $R^2$ |
|---|---|---|---|---|
| $Cr^{6+}$ | SD | 0.04369 | 0.02059 | 0.99002 |
| | Biochar (AC) | 0.03314 | 0.01818 | 0.99218 |

**Table 4:** Pseudo-second-order study for adsorption of Ni(II) on AC and SD

| Metal | Adsorbent | Intercept $Q_e$ | Slope $K_2$ | $R^2$ |
|---|---|---|---|---|
| $Ni^{2+}$ | SD | 0.1147 | 0.0153 | 0.99676 |
| | Biochar (AC) | 0.09493 | 0.01414 | 0.99845 |

and $Ni^{2+}$ (Figure 16). The variables Ce, $q_m$, and Kl were calculated for $Cr^{6+}$ (Table 5) and $Ni^{2+}$ (Table 6).

### 3.6.2 Freundlich isotherm study

The Freundlich adsorption isotherm model describes adsorption as a multilayer procedure, where the energy of active sites is distributed among various molecules that are already adsorbed. It was calculated using the following formula:

$$\ln q_e = \ln k_f + (l/n) \ln Ce \quad (6)$$

Here, Ce represents the amount of the remaining adsorbate in the solution ($mg \cdot L^{-1}$) at equilibrium, $K_f$ is the adsorption constant that indicates the adsorption capacity in $mg \cdot g^{-1}$, and $n$ is the adsorption intensity. The slope of the plot is equal to $1/n$, while the intercept corresponds to $K_f$. The values of $n$ and $K_f$ are determined by plotting ln $q_e$ versus ln Ce for Cr(VI) and Ni(II), as shown in Figures 17 and 18, and Table 7 ($Cr^{6+}$) and Table 8 ($Ni^{2+}$). The earlier analysis confirmed that the adsorption occurred via dynamic multilayer adsorption [43].

## 3.7 Thermodynamical analysis of Ni(II) and Cr(VI) adsorption

The Gibbs free energy ($\Delta G$), entropy ($\Delta S$), and enthalpy ($\Delta H$) values for the adsorption process were determined by

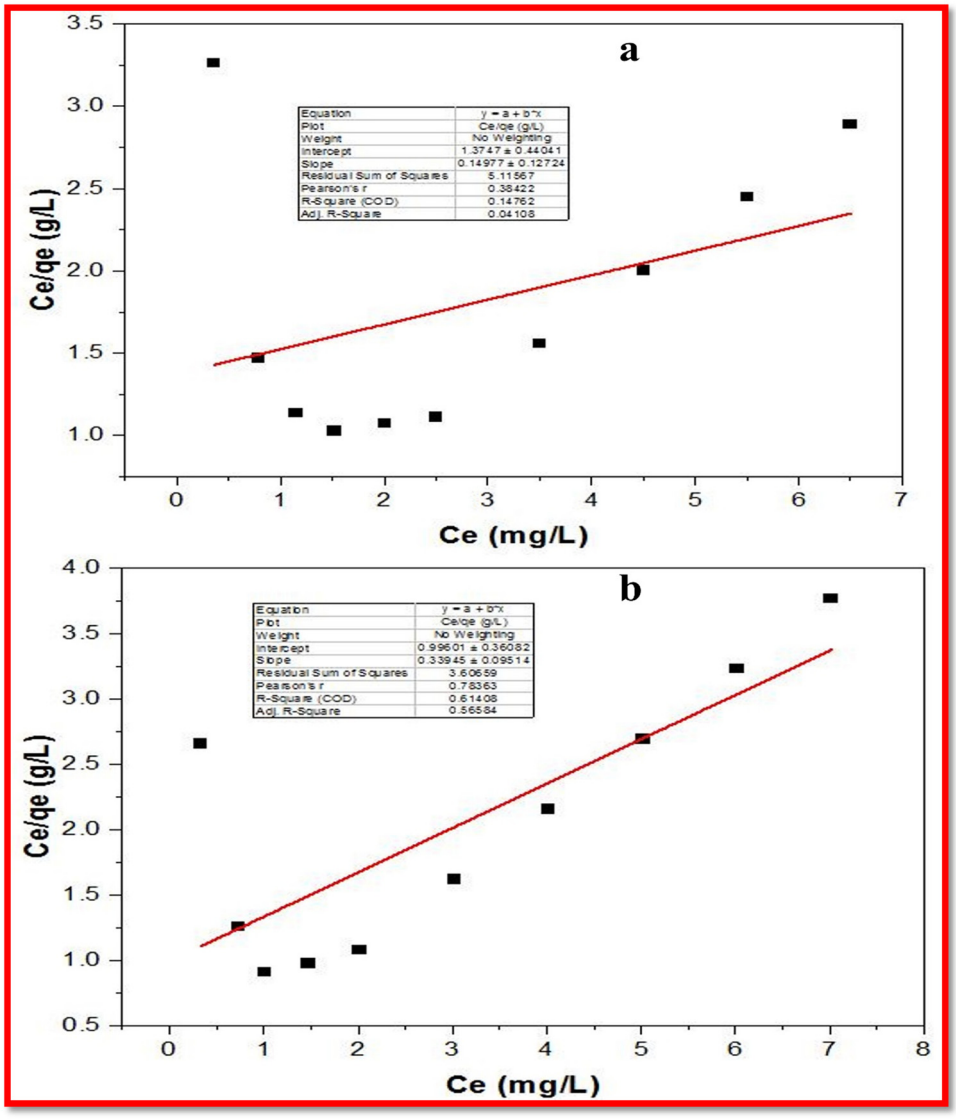


**Figure 15:** Langmuir isotherm model for $Cr^{6+}$ adsorption on SD (a) and AC (b).

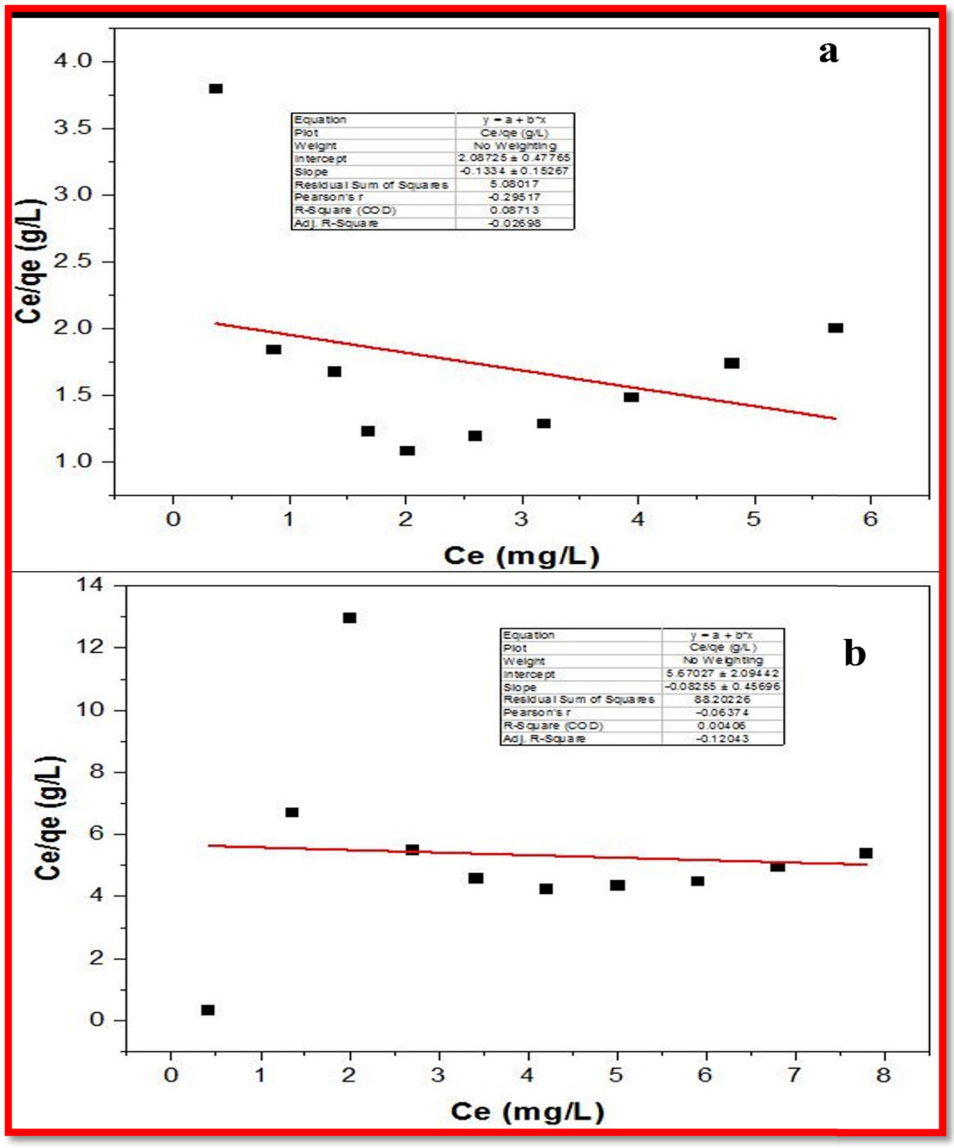


**Figure 16:** Langmuir adsorption model of $Ni^{+2}$ via (a) AC and (b) SD.

thermodynamic studies. The following equation was used to calculate the change in Gibbs free energy:

$$\Delta G = \Delta H - T\Delta S \tag{7}$$

A positive $\Delta H$ indicates endothermic chemosorption, which prefers higher temperatures, while a negative $\Delta H$ indicates exothermic physisorption, which favors lower temperatures.

The van't Hoff equation was applied to calculate the standard enthalpy change ($\Delta H°$) and standard entropy change ($\Delta S°$):

$$\ln k = \Delta S/R - \Delta H/RT \tag{8}$$

**Table 5:** Langmuir adsorption isotherm parameters for Cr(VI) adsorption on SD and AC

| Metal | Adsorbent | Intercept $Q_{max}$ (mg·g$^{-1}$) | Slope $b$ (L·mg$^{-1}$) | $R^2$ |
|---|---|---|---|---|
| $Cr^{6+}$ | SD | 1.3747 | −0.14977 | −0.04108 |
| | Biochar (AC) | 0.99601 | −0.33945 | −0.56584 |

**Table 6:** Langmuir adsorption isotherm parameters for Ni(II) on AC and SD

| Metal | Adsorbent | Intercept $Q_{max}$ (mg·g$^{-1}$) | Slope $b$ (L·mg$^{-1}$) | $R^2$ |
|---|---|---|---|---|
| $Ni^{2+}$ | SD | 5.67027 | −0.08255 | −0.12043 |
| | Biochar (AC) | 2.08725 | −0.1334 | −0.02698 |

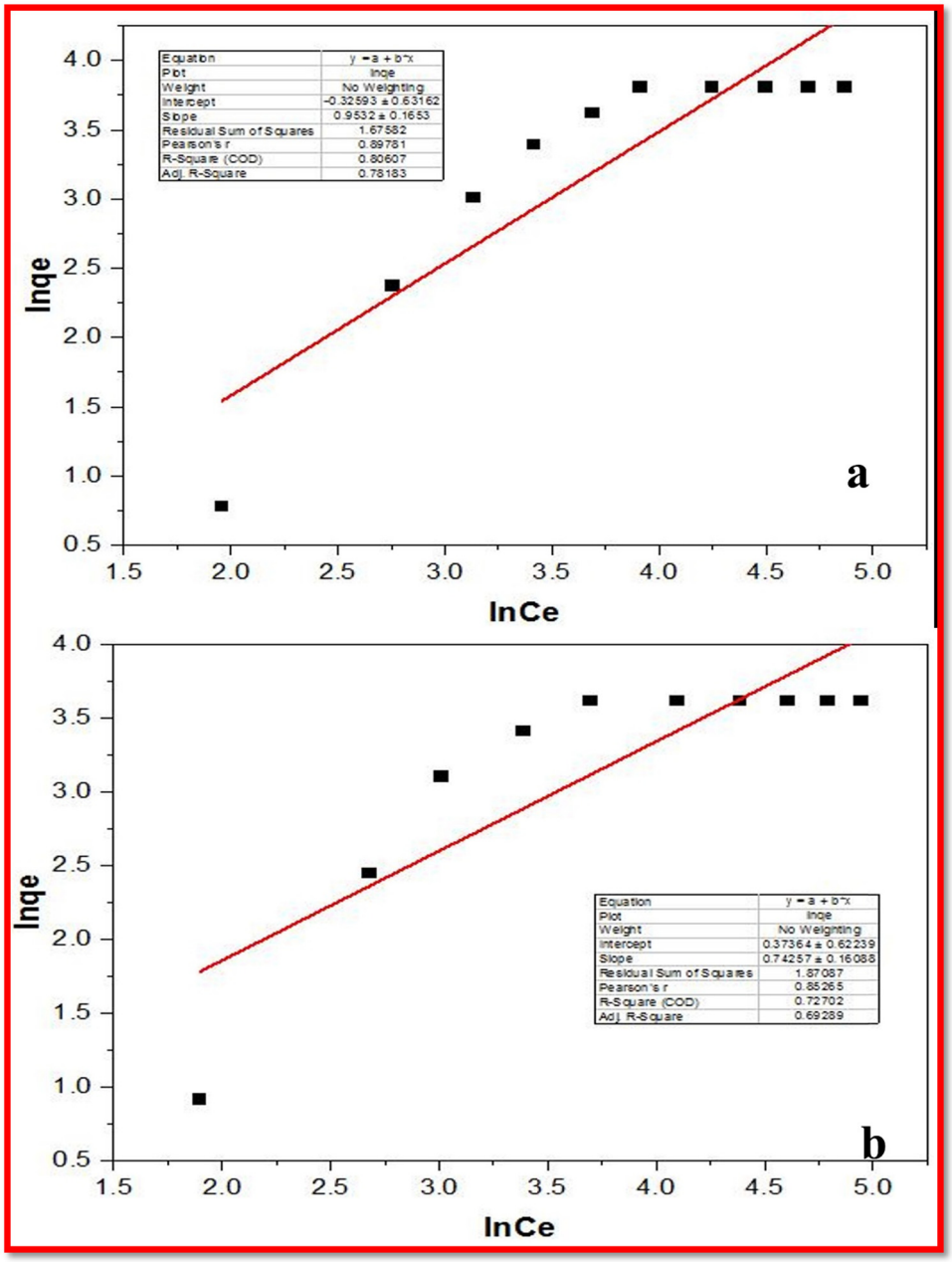


**Figure 17:** Plot of the Freundlich model for adsorption of Cr(VI) on SD (a) and AC (b).

where $R$ denotes the universal gas constant, and $T$ represents the Kelvin temperature. $\Delta H°$ and $\Delta S°$ for $Cr^{6+}$ and $Ni^{2+}$ were calculated from ln $K$ vs $1/T$ plots, as shown in Figures 19 and 20, and their values are shown in Tables 9 and 10. The negative $\Delta H°$ and positive $\Delta S°$ values indicate that the process is exothermic and spontaneous.

The negative value of $\Delta G$ for $Cr^{6+}$ metal in the table indicates spontaneous adsorption, while the negative $\Delta H$ value suggests exothermic physisorption at low temperatures. Negative $\Delta G$ values for $Ni^{2+}$ metal in the table indicate spontaneous adsorption, while negative $\Delta H$ values indicate exothermic physiosorption at low temperatures.

Despite the promising results observed in this study, there are several potential limitations that should be addressed in future research. The effectiveness of SD and AC at lower metal concentrations or in the presence of other competing contaminants need to be explored. Furthermore, while the batch experiments provided insights into adsorption kinetics and isotherms, the long-term stability,

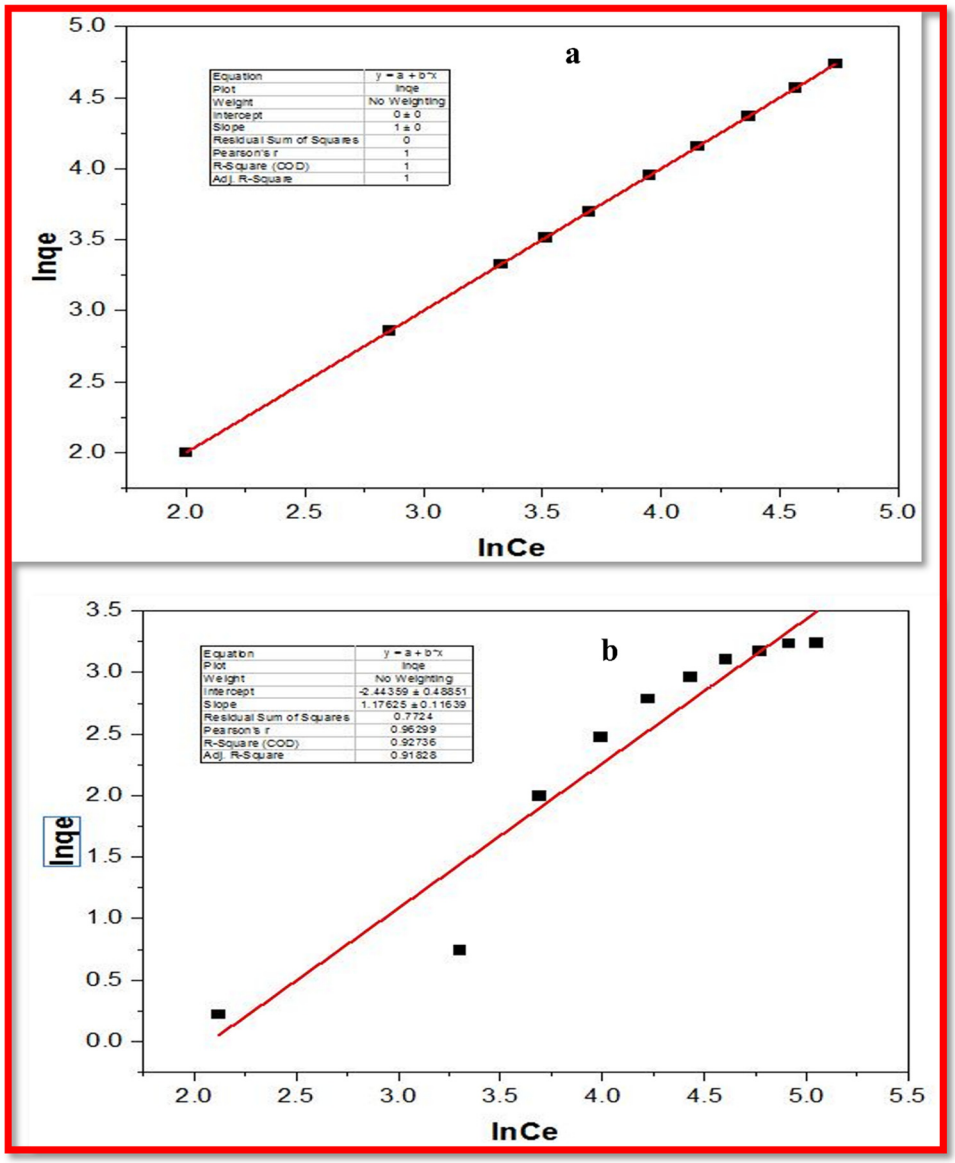


**Figure 18:** Freundlich model for adsorption of Ni(II) on SD (a) and AC (b).

**Table 7:** Freundlich isotherm parameters for $Cr^{+6}$ adsorption on SD and AC

| Metal | Adsorbent | Intercept $k_f$ | Slope 1/$n$ | $R^2$ |
|---|---|---|---|---|
| $Cr^{6+}$ | SD | −0.32593 | 0.9532 | 0.78183 = 0.8 |
| | Biochar (AC) | 0.37364 | 0.74257 | 0.69289 = 0.7 |

**Table 8:** Freundlich isotherm parameters for $Ni^{2+}$ adsorption onto SD and AC

| Metal | Adsorbent | Intercept $k_f$ | Slope 1/$n$ | $R^2$ |
|---|---|---|---|---|
| $Ni^{2+}$ | SD | 0 | 1 | 1 |
| | Biochar (AC) | −2.44359 | 1.17625 | 0.91828 |

regeneration potential, and reuse of the biosorbents were not investigated, which are critical factors for evaluating their practical applicability in large-scale water treatment systems. Finally, although the thermodynamic results suggest that the adsorption process is spontaneous and exothermic, scaling this process to real-world applications and assessing its economic feasibility are additional challenges that need to be explored.

Based on the findings of this study, it is essential for policymakers to promote the use of sustainable and cost-

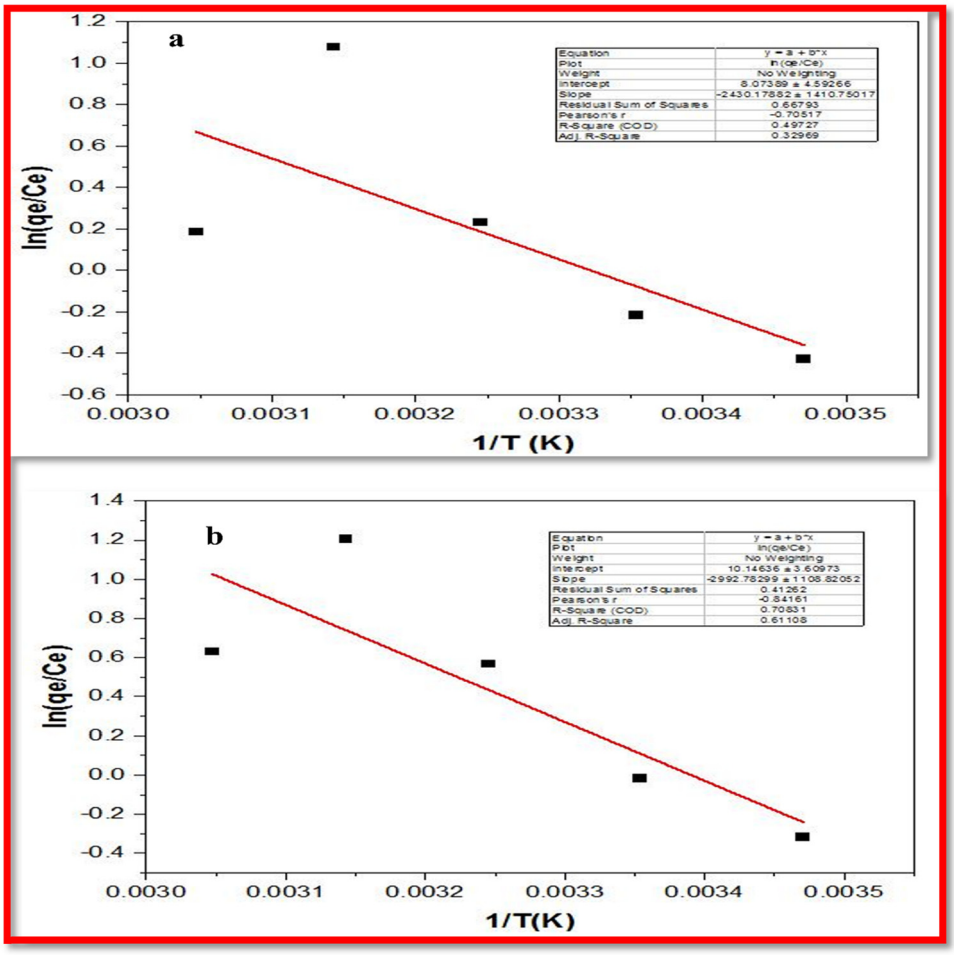


**Figure 19:** Thermodynamic investigation of Cr(VI) adsorption on SD (a) and AC (b).

effective water treatment methods, particularly in regions affected by heavy metal contamination. The successful application of *Prosopis glandulosa* raw SD and its derived biochar as adsorbents suggests a need for policies that encourage the development and implementation of low-cost, environmentally friendly technologies for water purification. Governments should consider supporting research into the scalability and regeneration of such biosorbents to ensure their long-term applicability. Additionally, policies could incentivize the use of natural, renewable materials like SD and biochar in water treatment industries to reduce dependency on harmful chemical treatments. Public/private partnerships could also be fostered to scale up the use of these materials in real-world water treatment systems, especially in communities facing critical issues with heavy metal contamination. Finally, regulatory frameworks should be established to ensure the safe disposal or reuse of biosorbents after their application, minimizing potential environmental impact and promoting a circular economy approach in water treatment practices.

# 4 Conclusion

The present study demonstrated the effective removal of potentially toxic elements, Cr(VI) and Ni(II), from aqueous solutions using *Prosopis glandulosa* raw SD and its derived biochar as adsorbents. The characterization of both materials confirmed their suitability for metal adsorption, and the batch experiments provided optimal conditions for maximum metal removal. The adsorption of Cr(VI) and Ni(II) was found to follow pseudo-second-order kinetics and the Freundlich adsorption isotherm model, indicating multilayer adsorption on the heterogeneous surface of the biosorbents. Thermodynamic analysis revealed that the adsorption process is spontaneous, exothermic, and therefore, favorable for practical applications in water treatment. The findings suggest that both SD and AC are highly effective, cost-efficient, and environmentally friendly materials for the removal of Cr(VI) and Ni(II) from contaminated water, offering a promising alternative for water purification technologies. A novel insight of this study is the identification of

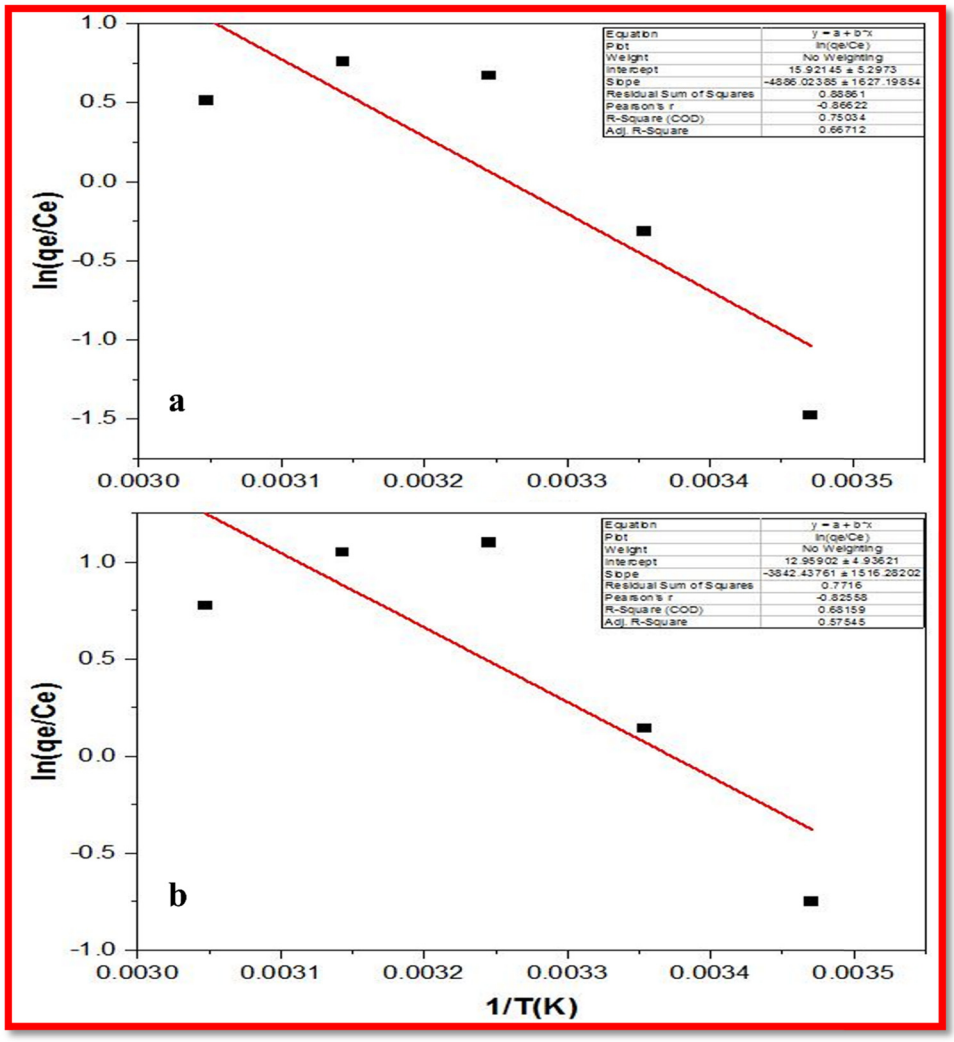


**Figure 20:** Thermodynamic investigation of Ni(II) on SD (a) and AC (b).

**Table 9:** Thermodynamic parameters for $Cr^{6+}$ adsorption on SD and AC prepared from *Prosopis glandulosa* stem

| Metal | Adsorbent | Intercept Δ*S* (J·mol$^{-1}$·K$^{-1}$) | Slope Δ*H* (J·mol$^{-1}$) | Δ*G* (J·mol$^{-1}$) | | | | | $R^2$ |
|---|---|---|---|---|---|---|---|---|---|
| | | | | 288 K | 298 K | 308 K | 318 K | 328 K | |
| $Cr^{6+}$ | SD | 8.073 | −2,430.2 | −475 | −484 | −492 | −499 | −508 | −0.329 |
| | Biochar (AC) | 10.15 | −2.993 | −293 | −303 | −313 | −323 | −333 | −0.611 |

**Table 10:** Thermodynamic parameters for $Ni^{+2}$ adsorption on SD and AC prepared from *Prosopis glandulosa* stem

| Metal | Adsorbent | Intercept Δ*S* (J·mol$^{-1}$·K$^{-1}$) | Slope Δ*H* (J·mol$^{-1}$) | Δ*G* (J·mol$^{-1}$) | | | | | $R^2$ |
|---|---|---|---|---|---|---|---|---|---|
| | | | | 288 K | 298 K | 308 K | 318 K | 328 K | |
| $Ni^{2+}$ | SD | 15.92 | −4,886 | −507 | −523 | −539 | −555 | −570 | 0.667 |
| | Biochar (AC) | 12.96 | −3,842 | −757 | −770 | −783 | −796 | −809 | 0.575 |

SD and AC as highly effective, sustainable, and low-cost materials for water remediation, providing a viable alternative to conventional methods for removing potentially toxic elements from water.

**Acknowledgments:** The authors extend their appreciation to the Researchers Supporting Project (number RSP2025R190), King Saud University, Riyadh, Saudi Arabia.

**Funding information:** The authors state that no funding was involved.

**Author contributions:** Sayed Muhammad Salman, Safina Razzaq, Muhammad Adnan, and Rozina: experiments, formal analysis, and writing. Wajid Zaman, Safina Razzaq: conceptualization, data curation, and formal analysis. Sayed Muhammad Salman, Dunia Abdel Aziz Al Farraj, Abdullah Ahmed Al-Ghamdi, Asif Kamal, Muhammad Adnan, Rozina, and Wajid Zaman: writing – review & editing, and investigation. Wajid Zaman, Sayed Muhammad Salman, Safina Razzaq, and Asif Kamal: characterization of fungus, data curation, and conceptualization. Hafiza Ayesha Rahim and Asif Kamal: conceptualization and formal analysis. Sayed Muhammad Salman, Jawher Alkahtani, and Moona Nazish: conceptualization and review & editing. Abdullah Ahmed Al-Ghamdi, Sabiha Sultana, and Dunia Abdel Aziz Al Farraj: funding, software, writing – review & editing, and formal analysis. Rozina, Abdullah Ahmed Al-Ghamdi, Sabiha Sultana, and Muhammad Adnan: conceptualization and data curation. Dunia Abdel Aziz Al Farraj and Sayed Muhammad Salman: designed experiments, resources, and supervision.

**Conflict of interest:** The authors state no conflict of interest.

**Data availability statement:** The datasets generated during and/or analyzed during the current study are available from the corresponding author on reasonable request.

# References

[1] Ullah I, Nuta FM, Levente D, Yiyu B, Yihan Z, Yi C, et al. Nexus between trade, industrialization, and marine pollution: A quantile regression approach. Ecol Indic. 2023;155:110992.

[2] Jadaa W, Mohammed H. Heavy metals–definition, natural and anthropogenic sources of releasing into ecosystems, toxicity, and removal methods–an overview study. J Ecol Eng. 2023;24(6):249–71.

[3] Mokhtaryan S, Khodabakhshi A, Sadeghi R, Nourmoradi H, Shakeri K, Hemati S, et al. New activated carbon derived from Gundelia tournefortii seeds for effective removal of acetaminophen from aqueous solutions: Adsorption performance. Arab J Chem. 2023;16(11):105253.

[4] Zhang P, Yang M, Lan J, Huang Y, Zhang J, Huang S, et al. Water quality degradation due to heavy metal contamination: Health impacts and eco-friendly approaches for heavy metal remediation. Toxics. 2023;11(10):828.

[5] Nivetha N, Srivarshine B, Sowmya B, Rajendiran M, Saravanan P, Rajeshkannan R, et al. A comprehensive review on bio-stimulation and bio-enhancement towards remediation of heavy metals degeneration. Chemosphere. 2023;312:137099.

[6] Aziz KHH, Mustafa FS, Omer KM, Hama S, Hamarawf RF, Rahman KO. Heavy metal pollution in the aquatic environment: efficient and low-cost removal approaches to eliminate their toxicity: a review. RSC Adv. 2023;13(26):17595–610.

[7] Mohapatra RK, Nayak M, Parhi PK, Pandey S, Thatoi H, Panda CR, et al. Biosorption performance and mechanism insights of live and dead biomass of halophilic Bacillus altitudinis strain CdRPSD103 for removal of Cd (II) from aqueous solution. Int Biodeterior & Biodegrad. 2024;191:105811.

[8] Shekhawat K, Chatterjee S, Joshi B. Chromium toxicity and its health hazards. Int J Adv Res. 2015;3(7):167–72.

[9] Mohanty S, Benya A, Hota S, Kumar MS, Singh S. Eco-toxicity of hexavalent chromium and its adverse impact on environment and human health in Sukinda Valley of India: A review on pollution and prevention strategies. Environ Chem Ecotoxicol. 2023;5:46–54.

[10] Iskandar IY, Gawkrodger DJ, Gittins M, Byrne L, Carder M, van Tongeren M. Trends in occupational and work-related contact dermatitis attributed to nickel, chromium and cobalt in the UK: findings from The Health and Occupation Research network 1996–2019. Br J Dermatology. 2024;190(5):751–7.

[11] Zaharia C, Musteret CP, Afrasinei MA. The use of coagulation–flocculation for industrial colored wastewater treatment – (I) the application of hybrid materials. Appl Sci. 2024;14(5):2184.

[12] Sheraz N, Shah A, Haleem A, Iftikhar FJ. Comprehensive assessment of carbon-, biomaterial-and inorganic-based adsorbents for the removal of the most hazardous heavy metal ions from wastewater. RSC Adv. 2024;14(16):11284–310.

[13] Agrahari S, Kumar S. Emerging and futuristic phyto-technologies for sustainable wastewater treatment with resource recovery and economical aspects. J Water Process Eng. 2024;65:105753.

[14] Sharma P, Chandra R. Phytoremediation mechanism and role of plant growth promoting rhizobacteria in weed plants for eco-restoration of hazardous industrial waste polluted site: a review. Environ Sci Pollut Res. 2024;31:1–26.

[15] Arbabi M, Hemati S, Shamsizadeh Z, Arbabi A. Nitrate removal from aqueous solution by almond shells activated with magnetic nanoparticles. Desalin Water Treat. 2017;80:344–51.

[16] Karimi M, Shirzad M, Silva JA, Rodrigues AE. Biomass/Biochar carbon materials for CO2 capture and sequestration by cyclic adsorption processes: A review and prospects for future directions. J $CO_2$ Util. 2022;57:101890.

[17] Gautam RK, Mudhoo A, Lofrano G, Chattopadhyaya MC. Biomass-derived biosorbents for metal ions sequestration: Adsorbent modification and activation methods and adsorbent regeneration. J Environ Chem Eng. 2014;2(1):239–59.

[18] Amer NM, Lahijani P, Mohammadi M, Mohamed AR. Modification of biomass-derived biochar: A practical approach towards development of sustainable CO2 adsorbent. Biomass Convers Biorefin. 2024;14(6):7401–48.

[19] Aziz S, Ali MI, Farooq U, Jamal A, Liu FJ, He H, et al. Enhanced bioremediation of diesel range hydrocarbons in soil using biochar made from organic wastes. Environ Monit Assess. 2020;192:1–14.
[20] Patel H. Batch and continuous fixed bed adsorption of heavy metals removal using activated charcoal from neem (Azadirachta indica) leaf powder. Sci Rep. 2020;10(1):16895.
[21] Johnson J, Mani J, Ashwath N, Naiker M. Potential for Fourier transform infrared (FTIR) spectroscopy toward predicting antioxidant and phenolic contents in powdered plant matrices. Spectrochim Acta Part A: Mol Biomol Spectrosc. 2020;233:118228.
[22] Liu Y, He Z, Uchimiya M. Comparison of biochar formation from various agricultural by-products using FTIR spectroscopy. Mod Appl Sci. 2015;9(4):246.
[23] Ahmad KF, Dar BA, Farooqui M. Characterization and adsorption of malachite green dye from aqueous solution onto Salix alba L. (Willow tree) leaves powder and its respective biochar. Int J Phytorem. 2023;25(5):646–57.
[24] Oraon A, Prajapati AK, Ram M, Saxena VK, Dutta S, Gupta AK. Synthesis, characterization, and application of microporous biochar prepared from Pterospermum acerifolium plant fruit shell waste for methylene blue dye adsorption: the role of surface modification by SDS surfactant. Biomass Convers Biorefin. 2024;14(1):931–53.
[25] Kumar M, Prasad D, Mondal MK. Adsorption analysis of Zn (II) removal from aqueous solution onto Argemone maxicana biochar. Biomass Convers Biorefin. 2023;13(5):4135–48.
[26] Singh M, Rano S, Roy S, Mukherjee P, Dalui S, Gupta GK, et al. Characterization of organophosphate pesticide sorption of potato peel biochar as low cost adsorbent for chlorpyrifos removal. Chemosphere. 2022;297:134112.
[27] Mishra RK, Mohanty K. Pyrolysis kinetics and thermal behavior of waste sawdust biomass using thermogravimetric analysis. Bioresour Technol. 2018;251:63–74.
[28] El-Sayed SA, Mostafa ME. Pyrolysis characteristics and kinetic parameters determination of biomass fuel powders by differential thermal gravimetric analysis (TGA/DTG). Energy Convers Manag. 2014;85:165–72.
[29] Venkatraman Y, Arunkumar P, Kumar NS, Osman AI, Muthiah M, Al-Fatesh AS, et al. Exploring modified rice straw biochar as a sustainable solution for simultaneous Cr (VI) and Pb (II) removal from wastewater: Characterization, mechanism insights, and application feasibility. ACS Omega. 2023;8(41):38130–47.
[30] Reddy AK, Jaisankar V. Adsorption treatment of heavy metal removal from simulated waste water using rice husk activated carbon (RHAC) and its polyvinylpyrrolidone (PVP) composite as an adsorbent. J Water Environ Sci. 2019;3(1):460–70.
[31] Ali NS, Khader EH, Abdulrahman MA, Salih IK, Albayati TM. Removal of anionic azo dye from wastewater using $Fe_3O_4$ magnetic nanoparticles adsorbents in a batch system. Desalin Water Treat. 2024;317:100033.
[32] Taqui SN, Syed AA, Mubarak NM, Farade RA, Khan MM, Kalam MA, et al. Insights into isotherms, kinetics, and thermodynamics of adsorption of acid blue 113 from an aqueous solution of nutraceutical industrial fennel seed spent. Sci Rep. 2023;13(1):22665.
[33] Olawale SA, Bonilla-Petriciolet A, Mendoza-Castillo DI, Okafor CC, Sellaoui L, Badawi M. Thermodynamics and mechanism of the adsorption of heavy metal ions on keratin biomasses for wastewater detoxification. Adsorpt Sci Technol. 2022;2022:1–13.
[34] Mahmoudian MH, Azari A, Jahantigh A, Sarkhosh M, Yousefi M, Razavinasab SA, et al. Statistical modeling and optimization of dexamethasone adsorption from aqueous solution by $Fe_3O_4$@NH2-MIL88B nanorods: Isotherm, kinetics, and thermodynamic. Environ Res. 2023;236:116773.
[35] Fakhar N, Khan SA, Siddiqi WA, Khan TA. Ziziphus jujube waste-derived biomass as cost-effective adsorbent for the sequestration of $Cd^{2+}$ from aqueous solution: isotherm and kinetics studies. Environmental. Nanotechnol Monit Manag. 2021;16:100570.
[36] Mwandira W, Nakashima K, Kawasaki S, Arabelo A, Banda K, Nyambe I, et al. Biosorption of Pb (II) and Zn (II) from aqueous solution by Oceanobacillus profundus isolated from an abandoned mine. Sci Rep. 2020;10(1):21189.
[37] Badsha MA, Khan M, Wu B, Kumar A, Lo IM. Role of surface functional groups of hydrogels in metal adsorption: From performance to mechanism. J Hazard Mater. 2021;408:124463.
[38] Dad FP, Sharif F, Nizami AS. Adsorption of trace heavy metals through organic compounds enriched biochar using isotherm adsorption and kinetic models. Environ Res. 2024;241:117702.
[39] Nnadozie EC, Ajibade PA. Adsorption, kinetic and mechanistic studies of Pb (II) and Cr (VI) ions using APTES functionalized magnetic biochar. Microporous Mesoporous Mater. 2020;309:110573.
[40] Herath A, Layne CA, Perez F, Hassan EB, Pittman Jr CU, Mlsna TE. KOH-activated high surface area Douglas Fir biochar for adsorbing aqueous Cr (VI), Pb (II) and Cd (II). Chemosphere. 2021;269:128409.
[41] Han Y, Cao X, Ouyang X, Sohi SP, Chen J. Adsorption kinetics of magnetic biochar derived from peanut hull on removal of Cr (VI) from aqueous solution: effects of production conditions and particle size. Chemosphere. 2016;145:336–41.
[42] Azizian S, Eris S, Wilson LD. Re-evaluation of the century-old Langmuir isotherm for modeling adsorption phenomena in solution. Chem Phys. 2018;513:99–104.
[43] Ma J, Hou L, Li P, Zhang S, Zheng X. Modified fruit pericarp as an effective biosorbent for removing azo dye from aqueous solution: study of adsorption properties and mechanisms. Environ Eng Res. 2022;27(2):200634.